The following publication M. Zhang, S. W. Or, S. Wang and F. -K. Chang, "Electromagnetic Navigation Linear Displacement Transducer Based on Magnetic Field Gradient Technique," in IEEE Transactions on Magnetics, vol. 51, no. 11, pp. 1-4, Nov. 2015, Art no. 8003204 is available at https://doi.org/10.1109/TMAG.2015.2440472.

Electromagnetic Navigation Linear Displacement Transducer Based on Magnetic Field Gradient Technique

Mingji Zhang[1], Siu Wing Or[1], *Senior Member, IEEE*, Sansheng Wang[2], and Fu-Kuo Chang[3]

[1]Department of Electrical Engineering, The Hong Kong Polytechnic University, Hung Hom, Kowloon, Hong Kong
[2]Department of Applied Physics, Beihang University, 100191, Beijing, China
[3]Department of Aeronautics and Astronautics, Stanford University, CA94305, USA

A linear displacement transducer (LDT) for electromagnetic navigation is developed based on the sensing of magnetic field gradients in a pair of counter-wound coils. The operation and linear response conditions of the LDT are theoretically described by electromagnetic formulations, numerically analyzed by COMSOL Multiphysics finite element analysis software, and experimentally verified in a 1/10-scaled inspection vehicle–overhead cable model. A high sensitivity of 51 μV/cm and a small nonlinearity of 3.7% are achieved in the LDT prototype by setting an optimal height-to-baseline h/L ratio of $1/\sqrt{8}$ in practical linear response condition with the transverse displacement d constraint of ±50% of L. The proposed LDT can overcome the discontinuous response and nonlinearity problems intrinsic in traditional magnetic field-based LDTs, thereby providing a continuous displacement (movement) feedback with an accuracy of within several millimeters.

***Index Terms*— counter-wound coils, electromagnetic navigation, linear displacement transducer, magnetic field gradients**

I. Introduction

ELECTROMAGNETIC navigation is a complementary guiding technique often used in navigation systems in conjunction with optical, visual, inertial, and global positioning navigations [1]–[4]. It is especially important for inspection vehicles or robots working in severe environments and requiring high levels of accuracy, stability, and cost-effectiveness. One of the most demanding applications is to navigate inspection vehicles along high-voltage overhead cables in electric power transmission networks, particularly for those distributed over complex landforms, large areas, and/or long distances [5]. In fact, long-term exposure of the overhead cables to outdoor environments with large temperature variations, high moisture and chemical contents, strong ultraviolet radiations, great mechanical stresses, etc. increases risks of insulation failures. If the potential and existing defects are not properly inspected and fixed, widespread blackouts may occur, leading to inestimable economic losses and grave social consequences [6].

To enable navigation capability in inspection vehicles, it is crucial to develop high-performance linear displacement transducers (LDTs) [7]. Currently, there are two major types of LDTs for electromagnetic navigation, namely sensing arrays and inductance comparators [8]–[10]. In sensing arrays, multiple Hall effect sensors or magnetic core inductors are arranged in an array form and used as the sensing elements to measure magnetic fields generated by the overhead cables [8], [11]. By optimizing the positions and responses of the sensing elements in the sensing arrays, the transverse displacements or movements of the inspection vehicles with respect to the overhead cables can be determined and then adjusted by the steering systems of the inspection vehicles [8]. By increasing the number of sensing elements in the sensing arrays, the navigation accuracy can be improved at the expense of reducing the navigation stability and increasing the cost of the navigation systems [12]. The nonlinearity caused by discrete signals from the sensing arrays also imposes challenges on the control algorithms [13], [14]. In inductance comparators, one referencing magnetic core inductor is designated to pick up ambient noise levels and several measuring magnetic core inductors are employed to acquire magnetic fields of the overhead cables [9], [11]. The transverse displacements of the inspection vehicles from the overhead cables are determined from the signal differences between the referencing and measuring magnetic core inductors so as to suppress ambient noises and improve the signal-to-noise ratios of the inductance comparators. However, the obtained transverse displacements are usually affected by the difference in hysteretic nonlinearity of the magnetic cores, which in turn increases the uncertainty in the response of the inductance comparators as well as the difficulty in the control of the inspection vehicles. These complexities have greatly impeded quantitative analyses of the effects of assembled and excitation parameters on the sensitivity, nonlinearity, etc. of this type of LDTs.

In this paper, we propose a new type of electromagnetic navigation LDT formed by a pair of coils counter-wound on a rod-shaped non-magnetic holder and served as a magnetic gradiometer to detect magnetic field gradients associated with the overhead cables. In contrast to traditional magnetic field-based, sensing array-type and inductance comparator-type LDTs, our magnetic field gradient-based, counter-wound coil-type LDT takes the distinct advantage of the dimensional difference in magnetic fields to determine magnetic field gradient-related transverse displacements with a minimization of far-field noises [15]. An electromagnetic model is theoretically established to describe the sensing principle of the LDT. The expression of output voltage as a function of both transverse displacement and assembled height is obtained by Faraday's law with a time derivative of the magnetic field gradient of the LDT. The theoretical and practical linear response conditions where the high-order residuals of voltage

Manuscript received 9, March, 2015. Corresponding author: Siu Wing Or (e-mail: eeswor@polyu.edu.hk).
Digital Object Identifier inserted by IEEE

response to transverse displacement are essentially zero and within ±50% of the baseline are found, respectively. Such findings are numerically analyzed and supported by COMSOL Multiphysics finite element analysis. With the guides of the theoretical and numerical designs, a LDT is prototyped and deployed in a 1/10-scaled inspection vehicle–overhead cable model to experimentally evaluate its sensitivity, nonlinearity, and errors between the theoretical, numerical, and experimental data at different combinations of transverse displacement and assembled height.

II. Magnetic Field Gradient-Based Electromagnetic Navigation Linear Displacement Transducer

In the following sections, the operation and linear response conditions of the proposed LDT are theoretically described by electromagnetic formulations (in Sec. IIA), numerically analyzed by COMSOL Multiphysics finite element analysis software (in Sec. IIB), and experimentally verified in a 1/10-scaled inspection vehicle–overhead cable model (in Sec. IIC).

A. Theoretical description

Figure 1 shows the assembly diagram and geometric configuration of the LDT, inspection vehicle, and overhead cable at a prescribed path of sensing and navigation. The inspection vehicle moves along the length of the overhead cable during navigation. The LDT, which consists of a pair of coils, namely coil l and coil 2, counter-wound on a rod-shaped Teflon holder with a baseline or a separation L, is installed in the front of the inspection vehicle with their lengths oriented in two orthogonal directions. There is a mechanism on the inspection vehicle for adjusting the assembled height h of the LDT toward the overhead cable.

In operation, a transverse displacement d of the inspection vehicle from the overhead cable distorts the geometric symmetry between coil 1–overhead cable and coil 2–overhead cable, resulting in different distances R_1 and R_2 as follows:

$$R_1 = \sqrt{h^2 + (0.5L - d)^2};\quad R_2 = \sqrt{h^2 + (0.5L + d)^2}. \quad (1)$$

The magnetic flux densities B_1 and B_2, as detected by coil 1 and coil 2, respectively, can be expressed as follows:

$$B_1 = \frac{h}{R_1}\frac{\mu_0 i}{2\pi R_1};\quad B_2 = \frac{h}{R_2}\frac{\mu_0 i}{2\pi R_2}, \quad (2)$$

where $\mu_0 = 4\pi \times 10^{-7}$ H/m is the permeability of free space and $i = \sqrt{2}I_{\text{rms}}\cos\omega t$ is the alternating current of the overhead cable with root-mean-square amplitude I_{rms} and angular frequency $\omega = 2\pi f$. The magnetic field gradient g of the LDT can be related to B_1, B_2, and L as

$$g = \frac{B_1 - B_2}{L}. \quad (3)$$

The output voltage V_{LDT} of the LDT can be derived from Faraday's law and related to g as

$$V_{\text{LDT}} = -nLA\frac{dg}{dt}, \quad (4)$$

where n and A are the number of turns and cross-section area of the counter-wound coils, respectively. By substituting Eqs. (1)–(3) into Eq. (4), the phasor amplitude of V_{LDT}, denoted as $\bar{V}_{\text{LDT}}$, can be obtained as

$$\bar{V}_{\text{LDT}} = \frac{\sqrt{2}nD^2\mu_0 I_{\text{rms}}\omega}{8}\left[\frac{h}{h^2+(0.5L-d)^2} - \frac{h}{h^2+(0.5L+d)^2}\right], \quad (5)$$

where D is the mean diameter of the counter-wound coils. In Eq. (5), d is the only dependent variable in the navigation process and can be minimized or even reset by adjusting the steering system of the inspection vehicle once $\bar{V}_{\text{LDT}}$ is detected by the LDT. Assuming the existence of a linear relationship between $\bar{V}_{\text{LDT}}$ and d in Eq. (5), it can be expanded by McLaurin series to be

$$\bar{V}_{\text{LDT}} = K\left[\frac{32hL}{(L^2+4h^2)^2}d\right] + \Delta, \quad (6)$$

where K is the sensitivity factor and Δ represents high-order residuals. Comparing Eqs. (5) and (6), K and Δ can be written, respectively, as

$$K = \sqrt{2}nD^2\mu_0 I_{\text{rms}}\omega \quad (7)$$

and

$$\Delta = K\left[\frac{h}{h^2+(0.5L-d)^2} - \frac{h}{h^2+(0.5L+d)^2} - \frac{32hL}{(L^2+4h^2)^2}d\right]. \quad (8)$$

For an effective navigation, it is required to constrain d in a reasonable operational range, say ±50% of L, as well as to satisfy the *theoretical* (*ideal*) linear response condition: $\Delta = 0$ in Eqs. (6) and (8). Accordingly, $\Delta = 0$ can now be released to become *practical* linear response condition: $\Delta|_{d=0.5L} = 0$ with an operation of d in the $\pm 0.5L$ range. By substituting $d = 0.5L$ into Eq. (8) and defining $p = h/L$ as the height-to-baseline ratio, we have

$$\Delta|_{d=0.5L} = \frac{K}{L}\left[\frac{1}{p} - \frac{p}{1+p^2} - \frac{16p}{(1+4p^2)^2}\right] = 0. \quad (9)$$

The solution to Eq. (9) is $p^2 = (h/L)^2 = 1/8$ or $p = h/L = 1/\sqrt{8}$. The solution gives the *optimal* h/L ratio for the successful realization of LDT in the *practical* linear response condition. From Eq. (7), the sensitivity of the LDT depends on the geometric properties (n and D^2) of the counter-wound coils and the characteristics of the alternating current (I_{rms} and ω). In practice, it may have a tradeoff between n and D in the design of a LDT with suitable size. To avoid the addition of the hysteretic nonlinearity effect in the LDT, magnetic cores are excluded from our counter-wound coils even though they could enhance the sensitivity of the LDT by concentrating magnetic fluxes from the overhead cable.

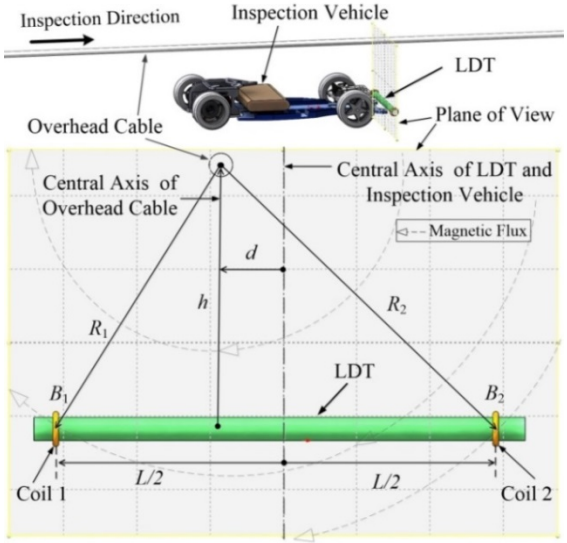

Fig. 1. Assembly diagram and geometric configuration of LDT, inspection vehicle, and overhead cable at a prescribed path of sensing and navigation.

B. Numerical analysis

To obtain an insight into the magnetic interaction between the overhead cable and the LDT, a three-dimensional dynamic simulation was implemented using magnetic field module available in COMSOL Multiphysics 5.0 finite element analysis (FEA) software. As illustrated in the inset of Fig. 2, the FEA model is meshed by 174,498 tetrahedral elements and consists of an air domain, an infinite domain, and three multi-turn coil domains. The overhead cable is modeled by a multi-turn coil domain with current excitation boundary condition. The cylindrical air domain is applied to the surrounding of the overhead cable domain with a higher mesh density to enable the computation of magnetic fields generated by the overhead cable. The cylindrical (hollow) infinite domain is added to the surrounding of the air domain to increase the computational accuracy. The LDT is modeled by two multi-turn coil domains with voltage computation boundary condition. The frequency and coil voltage computation solvers are used to compute the induced voltages of the counter-wound coils, as well as the magnetic field gradient and hence the output voltage of the LDT, in response to a parametric sweep of d of the inspection vehicle (also of the LDT) from the overhead cable.

Figure 2 shows the vector plot of the computed magnetic field distribution (the inset), together with the numerical and theoretical results of $\bar{V}_{\mathrm{LDT}}$ versus d, all at h = 6.4 cm, L = 18 cm, n = 400, D = 1.6 cm, I_{rms} = 5 A, and f = 60 Hz. It is noted that these h and L values fulfill the *optimal* h/L ratio requirement of $1/\sqrt{8}$ for the realization of LDT in the *practical* linear response condition: $\Delta|_{d=0.5L} = 0$ as described by Eq. (9) in Sec. IIA. The numerical and theoretical results reported here are determined under this optimal h/L ratio using the FEA model in Fig. 2 and Eq. (6) in Sec. IIA, respectively. It is clear that both numerical and theoretical plots exhibit good linear relationships between $\bar{V}_{\mathrm{LDT}}$ and d in the d range of ±9 cm (corresponding to ±50% of L) and with an extremely small error less than 0.5%. From the slopes of the plots, the sensitivity S_{LDT} and nonlinearity N_{LDT} of the LDT are found to 53 μV/cm and 0%, respectively.

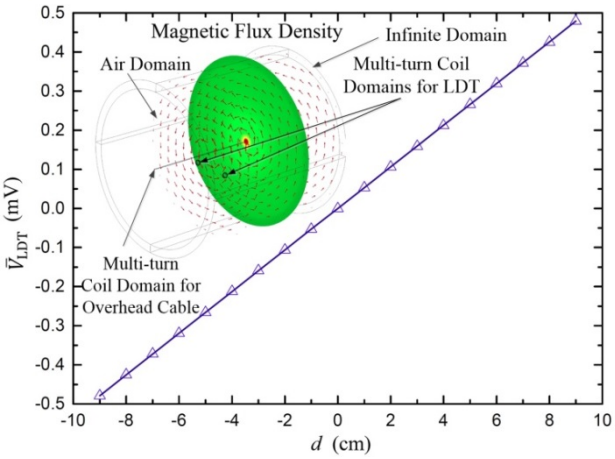

Fig. 2. Comparison between numerical (symbol) and theoretical (line) results of $\bar{V}_{\mathrm{LDT}}$ versus d under the *practical* linear response condition: $\Delta|_{d=0.5L} = 0$ with h = 6.4 cm and L = 18 cm ($h/L \approx 1/\sqrt{8}$). The inset is the FEA model and vector plot of the computed magnetic field distribution.

C. Experimental verification

To verify the theoretical and analytical designs in Secs. IIA and IIB, a LDT was prototyped in accordance with the assembled parameters (L = 18 cm, n = 400, and D = 1.6 cm) used to produce Fig. 2. As illustrated in Fig. 3, the LDT prototype was installed in the front of a 1/10-scaled inspection vehicle with their lengths oriented at two orthogonal directions as in Fig. 1. The inspection vehicle, together with the LDT prototype, was moved along the length of the overhead cable with different combinations of d and h settings of ±9 cm and 2–10 cm, respectively. An arbitrary waveform generator (Agilent-33210A) connected to a power supply amplifier operating in constant current mode (AE Techron 7548RLY) (not shown) were used to excite the overhead cable with an alternating current i having the same I_{rms} of 5 A and f of 60 Hz as those employed in Fig. 2. The output voltage $\bar{V}_{\mathrm{LDT}}$ of the LDT prototype was measured by a digitizing oscilloscope (Tektronix DPO2014) (not shown).

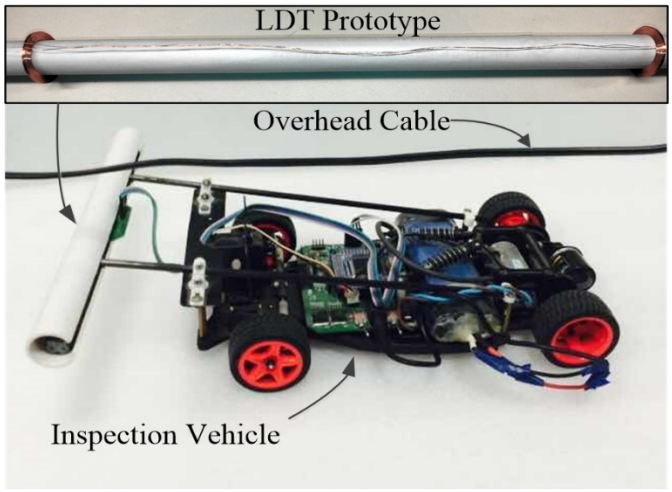

Fig. 3. LDT prototype and its 1/10-scaled inspection vehicle–overhead cable model.

Figure 4 shows the numerical and experimental $\bar{V}_{\mathrm{LDT}}$ as a function of d at different h when L = 18 cm, n = 400, D = 1.6 cm, I_{rms} =5 A, and f = 60 Hz. It is seen that the response of $\bar{V}_{\mathrm{LDT}}$ to d exhibits a high nonlinearity, which distorts the response curve from linear to S shape, at a small h of 2 cm. The nonlinearity decreases with increasing h, and the response curve becomes essentially linear at h = 6.4 cm. Beyond this critical h, the nonlinearity increases again, distorting the response curves even though the nonlinearity contribution is smaller compared to the cases with small h. The inset shows the errors between the experimental and numerical $\bar{V}_{\mathrm{LDT}}$. It is found that the experimental and numerical $\bar{V}_{\mathrm{LDT}}$ agree well with each other for different combinations of d and h. The maximum error is about 2% when d is close to ±0 cm. This error may be caused by measurements as a result of ambient noises, especially when the LDT prototype is working at a small g level.

In order to further investigate the sensitivity S_{LDT} and nonlinearity N_{LDT} of the LDT, the slopes of the experimental

$\bar{V}_{\mathrm{LDT}}$–d plots at different h in Fig. 4 are evaluated to construct the dependence of h on both S_{LDT} and N_{LDT} in Fig. 5. Two main observations are obtained. First, S_{LDT} decreases gradually from 175 to 26 μV/cm when h is increased from 2 to 10 cm. Second, N_{LDT} is minimized at h = 6.4 cm with a small value of 3.7%. The former observation can be explained by the use of a larger assembled height or vertical separation between the LDT (or the inspection vehicle) and the overhead cable, which in turn weakens the interaction of magnetic fields with the LDT. The latter observation can be understood by the fulfillment of the *optimal* h/L ratio requirement of $1/\sqrt{8}$ for the realization of the LDT in the *practical* linear response condition: $\Delta|_{d=0.5L} = 0$ as presented by Eq. (9) in Sec. IIA. Nonetheless, the experimental S_{LDT} and N_{LDT} of the LDT operating in the *practical* linear response condition with h = 6.4 cm and L = 12 cm are found to be 51 μV/cm and 3.7%, respectively. These imply the presence of millimeter-scale navigation accuracy in our LDT for use with most of steering control systems. In fact, the favorable performance can be further enhanced if ambient noises can be minimized and the LDT design can be improved.

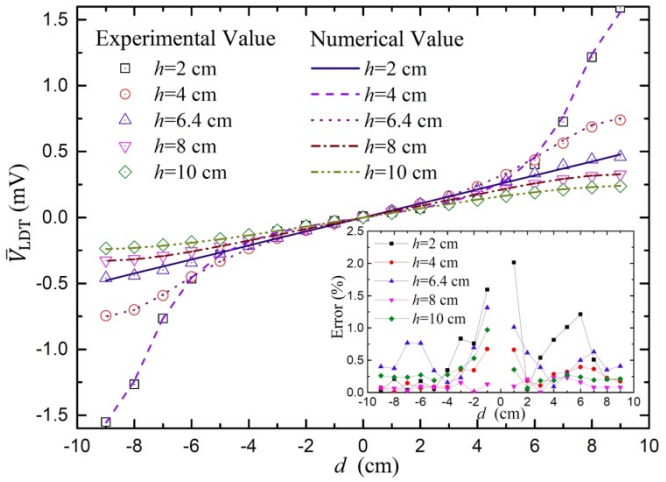

Fig. 4. Comparison between experimental (symbols) and numerical (lines) $\bar{V}_{\mathrm{LDT}}$ as a function of d at different h. The inset shows the errors between experimental and numerical $\bar{V}_{\mathrm{LDT}}$.

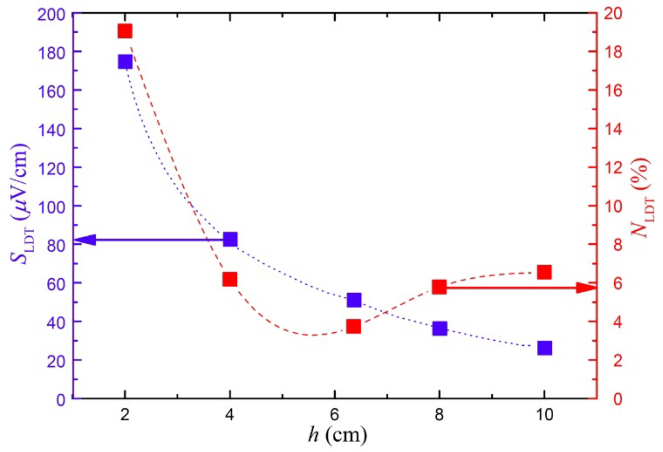

Fig. 5. Dependence of h on S_{LDT} and N_{LDT} obtained from the experimental $\bar{V}_{\mathrm{LDT}}$–d plots at different h in Fig. 4.

III. Conclusion

We have developed a simple and promising type of LDT for electromagnetic navigation based on magnetic field gradient sensing technique in a pair of counter-wound coils. The proposed LDT has been theoretically designed, numerically analyzed, and practically prototyped and deployed in a 1/10-scaled inspection vehicle–overhead cable model to evaluate its sensitivity, nonlinearity, and errors between the theoretical, numerical, and experimental data at different combinations of transverse displacement and assembled height. The high sensitivity of 51 μV/cm in conjunction with the small nonlinearity of 3.7% realized in the LDT prototype make it promise to enable continuous displacement feedback with millimeter-scale navigation accuracy in comparison with traditional magnetic field-based LDTs having discontinuous response and high level of nonlinearity.

Acknowledgments

This work was supported by the Research Grants Council of the HKSAR Government (PolyU 5228/13E) and The Hong Kong Polytechnic University (RTUY).

References

[1] S. Godha, S, "Performance evaluation of low cost MEMS-based IMU integrated with GPS for land vehicle navigation application," UCGE. Rep.20239t, Feb. 2006

[2] T. Chu, N. Guo, S. Backén, and D. Akos, "Monocular Camera/ IMU/ GNSS Integration for Ground Vehicle Navigation in Challenging GNSS Environments," *Sensors*, vol.12, no.3, pp. 3162-3185, Mar.2012.

[3] W. M. Hardesty, D. G. Caldwell and D. A. Cerchie, "Precision Multiple Vehicle Navigation System, " US Patent 20,150,025,797, Jan.2, 2015.

[4] G. S. Tewolde, "Sensor and network technology for intelligent transportation systems," in *Electro/Information Technology (EIT)*, IEEE International Conference on., 2012, pp.1-7.

[5] Y. Liu, Y. G. Wang, J. K. Xu and X. Z. Li, "Research and Design on Inspection Robot for High-Voltage Transmission Lines," *Advanced Materials Research*, vol.850, pp. 600-603, Dec. 2014.

[6] Y. Q. Liu, and Y. T. Liu, "Aspects on Power System Islanding for Preventing Widespread Blackout," in *IEEE International Conference on Networking, Sensing & Control*, 2006, pp.1090 - 1095.

[7] Y. G. Wang, H. D. Yu and J. K. Xu, "Design and Simulation on Inspection Robot for High-voltage Transmission Lines," *Automatic Control and Mechatronic Engineering*, vol. 615, pp.173-180, Aug. 2014.

[8] E. Jung, J. Kim, H. Cho, J. Lee and S. Kim, "Improvement of Position Accuracy of Magnetic Guide Sensor Using Kalman Filter," in *Intelligent Autonomous Systems* 12. Korea: Springer Berlin Heidelberg, 2013, pp. 817-824.

[9] J. Song, "Electromagnetic Induction Sensor of Navigation System for Spraying Robot," in *Proc. ICCE*, 2011, pp. 175-181.

[10] C. Y. Chan, "A system review of magnetic sensing system for ground vehicle control and guidance," California PATH Research Rep. UCB-ITS-PRR-2002-20, May. 2002.

[11] C. Walker, B. Armstrong, T. Bean, J. Canning, E. Wolbrecht, M. Anderson and D. Edwards, "Calibration and localization of AUV-acquired magnetic survey data, "in *Proc. OCEANS 2011, IEEE*. USA, 2011, pp.1-6.

[12] E. Wolbrecht, B. Gill, R. Borth, J. Canning, M. Anderson, and Edwards, D. "Hybrid Baseline Localization for Autonomous Underwater Vehicles," *Journal of Intelligent & Robotic Systems*, vol.78, no.3, pp. 1-19, Aug. 2014.

[13] R. Hennessy, F. Oppolzer, X. Fan, S. P. Singh and H. Durrant-Whyte, "System and method for autonomous navigation of a tracked or skid-steer vehicle," U.S. Patent No. 8,612,084. 17 Dec. 2013.

[14] Y. Liu, W. Zhang, X. Liu, and S. Qiu, "Study on electromagnetic navigation intelligent vehicle detection and control system," *Transducer and Microsystem Technologies*, vol.4, pp. 21, 2012.

[15] S. Tumanski, "Induction coil sensors—A review," *Measurement Science and Technology*, vol.18, no.3, pp. R31-R36, Mar, 2007.